Introduction to nonlinear optical spectroscopy

Eric Vauthey

Département de Chimie-Physique de l'Université de Genève, 30 Quai Ernest Ansermet, CH-1211 Genève 4 (http://www.unige.ch/sciences/chifi/Vauthey)
eric.vauthey@unige.ch

Content

1. Linear light-matter interactions

Light is an electromagnetic wave and many interactions with matter are due to its electric field component only. The propagation of light, and more precisely of its electric field, is described by a *wave equation*, derived from the well-known Maxwell equations of electromagnetism. In vacuum, this equation is expressed as :

$$\nabla^2 \vec{E} - \frac{1}{v_\phi^2} \frac{\partial^2 \vec{E}}{\partial t^2} = 0 \qquad (1.1)$$

where $\vec{E}$ is the electric field, ∇^2 is the Laplacien and v_ϕ is the phase velocity. In vacuum, v_ϕ is $v_\phi = c = (\mu_0 \varepsilon_0)^{-1/2}$ where μ_0 and ε_0 are the vacuum permeability and permittivity, respectively.

One evident solution of (1.1) is the harmonic wave :

$$\vec{E}(\vec{r},t) = \vec{A}\exp\left[i\left(\vec{k}\cdot\vec{r} - \omega\cdot t\right)\right] + c.c. = \vec{E}_0 \exp(-i\omega t) + c.c. \qquad (1.2)$$

where $\vec{A}$ is the amplitude of the wave and $\left(\vec{k}\cdot\vec{r} - \omega\cdot t\right)$ is its phase, $\vec{r}$ being the position vector and *t* is time. $\vec{k}$ is the wave vector (also called propagation vector) and points towards the direction of propagation of the wave. In vacuum, its magnitude is :

$$\left|\vec{k}\right| = k = \frac{2\pi}{\lambda} = \frac{\omega}{c} \qquad (1.3)$$

where λ is the wavelength and ω is the angular velocity $\omega = 2\pi\nu$, ν being the frequency. When applied on a material, an electric field polarises the molecules and creates an induced dipole moment, $\vec{\mu}_{ind} = e\vec{d}$, where $\vec{d}$ is the displacement and *e* the electronic charge. The macroscopic equivalent of the dipole moment is the polarisation, *P*:

$$\vec{P} = Ne\vec{d} \tag{1.4}$$

where N is the number of dipoles per unit volume.

As long as the electric field is weak, the polarisation is linearly proportional to the electric field , the proportionality constant being the electric (or optical) susceptibility, $\underline{\tilde{\chi}}$:

$$\vec{P} = \varepsilon_0 \underline{\tilde{\chi}} \cdot \vec{E} \tag{1.5}$$

$\underline{\tilde{\chi}}$ is a second rank tensor. The tilde indicates that this is a complex quantity. It relates the three cartesian coordinates of the polarisation with those of the electric field. The microscopic equivalent of $\underline{\tilde{\chi}}$ is the polarisability, $\underline{\tilde{\alpha}}$.

After the effect of an electric field on a material, one has now to consider the effect of a polarised material on the propagation of an electromagnetic wave. The wave equation for the propagation in a polarised material is :

$$\nabla^2 \vec{E} - \mu_0 \frac{\partial^2 \vec{D}}{\partial t^2} = 0 \tag{1.6}$$

where

$$\vec{D} = \varepsilon_0 \vec{E} + \vec{P} \tag{1.7}$$

After insertion of (1.5) and (1.7) in (1.6), the wave equation becomes :

$$\nabla^2 \vec{E} - \mu_0 \varepsilon_0 (1 + \underline{\tilde{\chi}}) \frac{\partial^2 \vec{E}}{\partial t^2} = 0 \tag{1.8}$$

By comparing with equation (1.1), one obtains the phase velocity in the material : $\tilde{v}_\phi = \left[\mu_0 \varepsilon_0 (1 + \tilde{\chi})\right]^{-1/2}$.

The optical susceptibility is usually expressed in terms of the complex refractive index, $\tilde{n}$:

$$\tilde{n} = \frac{v_\phi(vacuum)}{\tilde{v}_\phi(mat.)} = (1 + \tilde{\chi})^{1/2} \tag{1.9}$$

$\tilde{n}$ is usually split into a real and an imaginary parts :

$$\tilde{n} = n + iK \tag{1.10}$$

where n is the refractive index. This index is also defined as :

$$n = \frac{c}{v_\phi} \tag{1.11}$$

v_ϕ being the phase velocity in the material (the real part of $\tilde{v}_\phi$). The effect of n on the light is the modification of the phase velocity.

The second term in (1.10), K, is called attenuation constant. It accounts for the effect of the material on the amplitude of the wave, hence on its intensity. This corresponds to the absorption of light.
The relationship between K and the absorbance $\mathcal{A}$ is :

$$K = \frac{\ln 10 \ \mathcal{A}\lambda}{4\pi L} \tag{1.12}$$

where L is the pathlength in the material.

K and n are related by a Kramers-Kronig relationship :

$$n(\omega) = -\frac{1}{\pi}\int \frac{K(\omega')}{(\omega - \omega')} d\omega' \tag{1.13}$$

In a microscopic picture, absorption and index of refraction can be understood by considering that the incoming optical field creates an induced dipole moment on the molecules. If the optical field oscillates at a resonance frequency of the molecules, this induced dipole moment corresponds to a solution of the time-dependent Schrödinger

equation. This dipole (called the transition dipole) can exchange energy with the optical field, leading to absorption or emission.

If the induced dipole moment does not not oscillate at a resonance frequency, no energy exchange with the field is possible. The dipole simply reemits an electric field at the same frequency. This effect is at the origin of the refractive index.

2. Optical susceptibility at high light intensity

In principle, all the optical properties of a material and the corresponding phenomena (absorption, emission, refraction, reflection, scattering, ...) are accounted for by the susceptibility $\underline{\tilde{\chi}}$. When the light intensity is small, this susceptibility is independent of the electric field, hence of the intensity ($I \propto |E^2|$).

However, when the electric field is very intense, the optical susceptibility depends on the electric field. In this case, the polarisation can be expressed as a power series of the electric field :

$$\vec{P} = \vec{P}^{L} + \vec{P}^{NL} = \varepsilon_0 \left[\underline{\chi}^{(1)} \cdot \vec{E} + \underline{\chi}^{(2)} \cdot \vec{E} \cdot \vec{E} + \underline{\chi}^{(3)} \cdot \vec{E} \cdot \vec{E} \cdot \vec{E} \right] \qquad (2.1)$$

where $\underline{\chi}^{(1)}$ is the linear optical susceptibility and corresponds to the susceptibility at low intensity. $\underline{\chi}^{(2)}$ is the second order nonlinear optical susceptibility and is a third rank tensor. It contains 27 elements, which correspond to the possible combinations of the three cartesian coordinates of the polarisation and of the two interacting electric fields. $\underline{\chi}^{(3)}$ is the third order nonlinear optical susceptibility and is a fourth rank tensor with 3^4 elements. These tensors can be complex quantities but the tilde has been omitted for simplicity.

The order of magnitude of the elements of $\underline{\chi}^{(1)}$ is 1, that of the elements of $\underline{\chi}^{(2)}$ is 10^{-12} m/V and that of $\underline{\chi}^{(3)}$ is 10^{-23} m^2/V^2. Therefore, a nonlinear relationship between the polarisation and the electric field appears only with strong fields.

Such fields can be found in laser pulses. The relationship between the light intensity *I* and the electric field is :

$$I = 2n \left(\frac{\varepsilon_0}{\mu_0} \right)^{1/2} \left| \vec{E}_0 \right|^2 \qquad (2.2)$$

Some numerical examples are illustrated in the following table :

I (W/m^2)	10^4	10^7	10^{10}	10^{13}	10^{16}
E (V/m)	$1.37 \cdot 10^3$	$4.34 \cdot 10^4$	$1.37 \cdot 10^6$	$4.34 \cdot 10^7$	$1.37 \cdot 10^9$

Such intensities can be achieved by focusing laser pulses. For example, the light intensity in a 10 ns, 1 mJ pulse focused to a spot of 10 µm diameter amounts to 0.3 GW/cm^2. With pulses of 100 fs duration, this intensity is reached with an energy of 10 nJ/pulse only.

These intense optical pulses allow the generation of electric fields as large as those existing between the charges, nuclei and electrons, which constitute matter. Therefore, the optical properties of the material are modified.

One could say that $\underline{\chi}^{(2)}$ represents the variation of the optical susceptibility with the electric field :

$$\chi^{(2)} \approx \frac{\partial \chi}{\partial E} \tag{2.3}$$

As the polarisation and the electric field are vectors, the component of the nonlinear susceptibility along a cartesian coordinate is expressed as :

$$P_i^{(2)} = \varepsilon_0 \sum_{j,k=1}^{3} \chi_{ijk}^{(2)} E_j E_k \tag{2.4}$$

where i,j,k are the cartesian coordinates, i represents the polarisation component, j and k are the directions of the polarisation planes of the two electric fields and $\chi_{ijk}^{(2)}$ is one of the 27 tensors elements of $\underline{\chi}^{(2)}$.

The microscopic equivalent of $\underline{\chi}^{(2)}$ is $\underline{\beta}$, the second order hyperpolarisability and that of $\underline{\chi}^{(3)}$ is $\underline{\gamma}$, the third order hyperpolarisability.

The polarisation can be expressed in terms of these microscopic quantities :

$$\vec{P} = \varepsilon_0 N\left[\underline{\alpha}\cdot\vec{E}_{loc} + \underline{\beta}\cdot\vec{E}_{loc}\cdot\vec{E}_{loc} + \underline{\gamma}\cdot\vec{E}_{loc}\cdot\vec{E}_{loc}\cdot\vec{E}_{loc}\right] \qquad (2.5)$$

where $\vec{E}_{loc}$ is the local field. The latter is different from the external electric field, $\vec{E}$, because of the material contribution. Indeed, the local field is :

$$\vec{E}_{loc} = \vec{E} + \vec{E}_{sph} = \vec{E} + \frac{1}{3\varepsilon_0}\vec{P} \qquad (2.6)$$

where $\vec{E}_{sph}$ is the field induced by a dielectric of the surface of a spherical cavity. Expressing $\vec{P}$ with (2.1) and neglecting the nonlinear terms, one obtains :

$$\vec{E}_{loc} = \vec{E} + \frac{1}{3}\chi^{(1)}\vec{E} \qquad (2.7)$$

Using the relationship between the susceptibility and the relative dielectric constant, ε, $\chi = \varepsilon - 1$, the local field is :

$$\vec{E}_{loc} = \left(\frac{\varepsilon + 2}{3}\right)\vec{E} = f_L\vec{E} \qquad (2.8)$$

where f_L is the Lorentz local field correction factor.

3. Generation of new frequencies

Let's consider a radiation field oscillating at ω_1 and ω_2 and propagating along z. Its electric field can be described as :

$$E(t) = A_1\cos(\omega_1\cdot t + k_1 z) + A_2\cos(\omega_2\cdot t + k_2 z) \qquad (3.1)$$

If one takes a material with a non vanishing nonlinear susceptibility $\underline{\chi}^{(2)}$, the nonlinear polarisation ($\vec{P}^{(2)} = \underline{\chi}^{(2)} \cdot \vec{E} \cdot \vec{E}$) depends on the square of the electric field. The square of (3.1) at z=0 is :

$$E^2(t) = A_1^2 \cos^2(\omega_1 t) + A_2^2 \cos^2(\omega_2 t) + 2A_1 A_2 \cos(\omega_1 t)\cos(\omega_2 t) \qquad (3.2)$$

Using the following relationship :

$$\cos^2\alpha = \frac{1}{2} + \frac{1}{2}\cos 2\alpha \qquad \text{and} \qquad \cos\alpha\cos\beta = \frac{1}{2}\cos(\alpha+\beta) + \frac{1}{2}\cos(\alpha-\beta)$$

(3.2) becomes :

$$E^2(t) = \frac{1}{2}\left(A_1^2 + A_2^2\right) + \frac{1}{2}A_1^2\cos(2\omega_1 t) + \frac{1}{2}A_2^2\cos(2\omega_2 t) + A_1A_2\left\{\cos\left[(\omega_1+\omega_2)t\right] + \cos\left[(\omega_1-\omega_2)t\right]\right\}$$

This new electric field contains a time independent term, terms oscillating at the double frequencies, $2\omega_1$ and $2\omega_2$, as well as term oscillating at the sum frequency, $\omega_1+\omega_2$, and at the difference frequency $|\omega_1 - \omega_2|$.

Consequently, the polarisation oscillates at these frequencies as well and is the source of electromagnetic waves at these very same frequencies (vide infra).

All these frequencies are not produced simultaneously. The creation of a wave at one of them requires well-defined conditions, the phase-matching conditions, that we will discuss later.

The phenomenon where $2\omega_1$ and $2\omega_2$ frequencies are produced is called *second harmonic generation* (SHG). This effect is intensively used in laser spectroscopy laboratories. For example, with a Nd:YAG laser oscillating at 1064 nm (near IR), SHG produces light at 532 nm (green).

For the frequency at $\omega_1+\omega_2$, one speaks about *sum frequency generation* (SFG). With a Nd:YAG laser, one can thus obtain light at 355 nm by mixing light at 532 nm and 1064 nm. This process is also used to convert a weak light signal from ω_1 to ω_3 by mixing it with a laser beam at ω_2. This technique is called *up-conversion*.

The build up of light at $|\omega_1 - \omega_2|$ is called *difference frequency generation* (DFG) or mixing (DFM). This process is used to generate coherent light in the infrared by mixing two laser beams at close frequencies. (Ex : 532 nm and 600 nm → 4700 nm (2100 cm^{-1})).
The process where a polarisation at frequency zero is obtained is called *optical rectification* (OR). In this case, the polarisation follows the amplitude of the electric field. If one uses an optical pulse, the time profile of the polarisation will be the same as the time profile of the pulse envelope of the related electric field. This technique can be used to generate optical radiation in the THz regime with visible ultrashort laser pulses.
These phenomena are often illustrated using energy level diagrams involving so-called « virtual » transition. (cf. **Figure 3.1**).

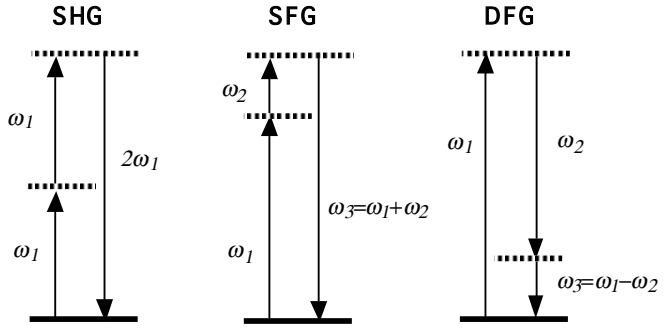

Figure 3.1: energy level representation of frequency conversion processes.

For a better understanding of the generation of new frequency, one has to consider the propagation of an electromagnetic wave in a material with a nonlinear polarisation :

$$-\nabla^2 \vec{E} + \frac{\underline{\varepsilon}^{(1)}(\omega)}{c^2} \cdot \frac{\partial^2 \vec{E}}{\partial t^2} = -\mu_0 \frac{\partial^2 \vec{P}^{NL}}{\partial t^2} \qquad (3.3)$$

where the linear polarisation is included in the dielectric tensor $\underline{\varepsilon}^{(1)}(\omega) = \varepsilon_0\left(1 + \underline{\chi}^{(1)}(\omega)\right)$.
The term on the r.h.s. of (3.3) acts as a source of new radiations.

For frequency conversion, this equation has to be simultaneously valid for all the waves involved. We will consider the SFG in more detail. In this case, two waves at ω_1 and ω_2

interact in a material to generate a new wave at ω_3. To simplify the notation, we will work with scalar quantities and assume that all three waves travel along z.
The electric fields are described as :

$$E_j(z,t) = E_{j,0}\exp\left(-i\omega_j t\right) + c.c. \qquad j=1,2,3 \tag{3.4}$$

with

$$E_{j,0} = A_j \exp(ik_j z) \qquad j=1,2,3 \tag{3.5}$$

The nonlinear polarisation in (3.3) is expressed as :

$$P^{NL}(z,t) = P_3\exp\left(-i\omega_3 t\right) + c.c. \tag{3.6}$$

where the amplitude P_3 is given by :

$$P_3 = 2\varepsilon_0\chi^{(2)}E_{1,0}E_{2,0} = 2\varepsilon_0\chi^{(2)}A_1A_2\exp\left[i\left(k_1+k_2\right)z\right] \tag{3.7}$$

The factor two accounts for the number of possible permutations of the fields 1 and 2. If one inserts (3.4) to (3.7) in the wave equation (3.3), one gets :

$$\begin{aligned}&\left[\frac{\partial^2 A_3}{\partial z^2} + 2ik_3\frac{\partial A_3}{\partial z} - k_3^2 A_3 + \frac{\varepsilon^{(1)}(\omega_3)\omega_3^2 A_3}{c^2}\right]\exp\left[i\left(k_3 z-\omega_3 t\right)\right] + c.c.\\ &= -\frac{2\chi^{(2)}\omega_3^2}{c^2}A_1A_2\exp\left[i\left(\left(k_1+k_2\right)z-\omega_3 t\right)\right] + c.c.\end{aligned} \tag{3.8}$$

As $k_3^2 = \varepsilon^{(1)}(\omega_3)\omega_3^2/c^2$, the third and fourth terms as well as the c.c. on the l.h.s. of (3.8) cancel. One devides by $\exp\left[i\left(k_3 z-\omega_3 t\right)\right]$ and obtains :

$$\frac{d^2A_3}{dz^2} + 2ik_3\frac{dA_3}{dz} = -\frac{2\chi^{(2)}\omega_3^2}{c^2}A_1A_2\exp\left[i\left(k_1+k_2-k_3\right)z\right] \tag{3.9}$$

The first term on the l.h.s. is usually neglected because it is much smaller than the second. This simplification implies that the variation of A_3 over a distance equal to a wavelength is negligibly small. This is called *the slowly varying envelope approximation*. Thus equation (3.9) becomes :

$$\frac{dA_3}{dz} = \frac{i\chi^{(2)}\omega_3^2}{k_3 c^2} A_1 A_2 \exp(i\Delta k z) \tag{3.10}$$

where $\Delta k = k_1 + k_2 - k_3$.

This equation is called *coupled amplitudes* equation, because it shows how the amplitude at ω_3 varies upon coupling with the waves at ω_1 and ω_2. To get the spatial dependence of the amplitudes of these two waves, one has to repeat the same procedure by inserting equation (3.4) with j=1 or 2 in equation (3.3). This gives two new coupled equations.

At the output of the material, the amplitude of the wave at ω_3 is given by the integral of equation (3.10) from z=0 to z=L, where L is the optical pathlength in the material. If Δk=0, one obtains :

$$A_3(L) = \frac{i\chi^{(2)}\omega_3^2 A_1 A_2}{k_3 c^2} L \tag{3.11a}$$

and if $\Delta k \neq 0$:

$$A_3(L) = \frac{i\chi^{(2)}\omega_3^2 A_1 A_2}{k_3 c^2} \int_0^L \exp(i\Delta k z) dz = \frac{i\chi^{(2)}\omega_3^2 A_1 A_2}{k_3 c^2} \left(\frac{\exp(i\Delta k L) - 1}{i\Delta k} \right) \tag{3.11b}$$

As the intensity is proportional to the square of the amplitude $\left(I_j = 2n_j (\varepsilon_0 / \mu_0)^{1/2} |A_j|^2 \right)$, I_3: is :

$$I_3 = \frac{\mu_0^{1/2} \omega_3^2 |\chi^{(2)}|^2 I_1 I_2}{2\varepsilon_0^{1/2} n_1 n_2 n_3 c^2} L^2 \tag{3.12a}$$

or

$$I_3 = \frac{\mu_0^{1/2} \omega_3^2 |\chi^{(2)}|^2 I_1 I_2}{2\varepsilon_0^{1/2} n_1 n_2 n_3 c^2} L^2 \, \mathrm{sinc}^2(\Delta k L / 2) \tag{3.12b}$$

with sinc(x)=sin(x)/x.

In the above derivation, the amplitude of the waves at ω_1 and ω_2 was assumed to be unaffected by the nonlinear interaction. This is only valid in the case of a conversion with small efficiency. In the opposite case, the mathematical description is more complex.

Equation (3.12a) shows that if Δk=0, the intensity of the new wave increases with the square of the interaction length.

The physical meaning of Δk=0 is the conservation of momentum ($\hbar k = p$). One can also says that at Δk=0, there is a phase matching between the incoming waves and the new wave. In the case of SHG, the wave at ω_1 at position z generates a polarisation at $2\omega_1$. Thus at z, a wave at $2\omega_1$ is created. This process continues as the wave at ω_1 propagates in the material. In order for the new $2\omega_1$ wave to build up, its phase has to be perfectly synchronised with that of the ω_1 wave over the whole length of the material, L. If this is not the case, the $2\omega_1$ wave generated at z can interferes destructively with that created at $z+\Delta z$. Hence its intensity will decrease.

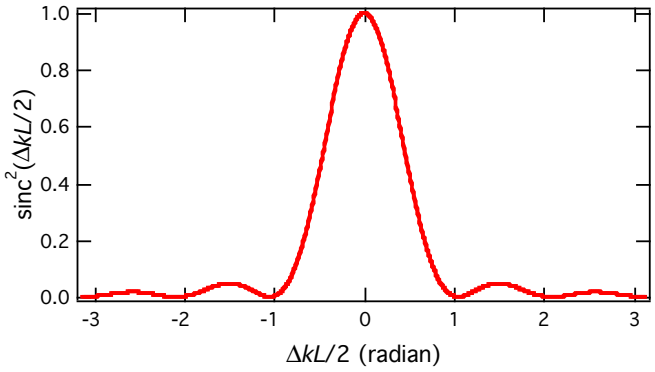

Figure 3.2: effect of the phase mismatch on the SHG efficiency.

If the three waves are collinear, the phase matching condition implies that :

$$k_3 = k_1 + k_2 \qquad (3.13a)$$

or, as $k = n\omega / c$,

$$n_3\omega_3 = n_1\omega_1 + n_2\omega_2 \qquad (3.13b)$$

For SHG, $\omega_1=\omega_2$ and thus: $n_3 = n_1$ (3.13c)

If the frequencies are far from an absorption band of the material, the refractive index increases with the frequency (normal dispersion). Consequently, $n_3>n_1$ and the phase matching condition cannot be fulfilled.

Mathematically, the effect of phase mismatch is accounted for by the sinc function in equation (3.11b). **Figure 3.2** shows the shape of this function. One can see that the conversion efficiency depends on the relative magnitude of Δk and L. One can define a coherence length, $L_c=2/\Delta k$. If Δk is small, the two waves remains more or less in phase over a relatively long distance, i.e. the coherence length is large. Consequently, if the material thickness is smaller than L_c, the conversion can be efficient.

As an example, let's take a nonlinear material like KDP (potassium (dihydrogenophosphate). This is an uniaxial crystal, whose ordinary refractive index is :

$$n_o^2 = 2.259276 + \frac{0.01008956}{\lambda^2 - 0.0112942625} + \frac{13.00522\lambda^2}{\lambda^2 - 400} \qquad (3.14)$$

At 1.064 μm, the ordinary refractive index amounts to 1.4938 and that at 0.532 μm is 1.5124. Therefore, the phase mismatch is $2.2\text{x}10^5$ m^{-1} and the coherence length is L_c=9 μm. This means that if one wants to generate 532 nm light by SHG, the crystal thickness has to be smaller than 9 μm. In this case, the efficiency of SHG is inferior by a factor $8\text{x}10^{-7}$ to the efficiency that would be achieved with a 1 cm crystal, assuming Δk=0.

In order to fulfill the phase matching condition for process based on second order nonlinearity, one uses birefringent materials.

For example, an uniaxial crystal is characterised by a refractive index n_z for light polarised along the optical axis z, and by a refractive index $n_x=n_y$ for light polarised along x and y. An electromagnetic wave with the polarisation plane in the xy plane experiences the refractive index $n_x=n_y$, called ordinary refractive index, n_o. On the other hand, if the polarisation plane is in the planes xz or yz , the wave feels a refractive index between $n_x=n_y$ and n_z, depending on its direction of propagation relatively to the optical axis of the

crystal. This refractive index is called extraordinary refractive index. The refractive index of such uniaxial crystal can be represented by an ellipsoid (see **Figure 3.3A**).

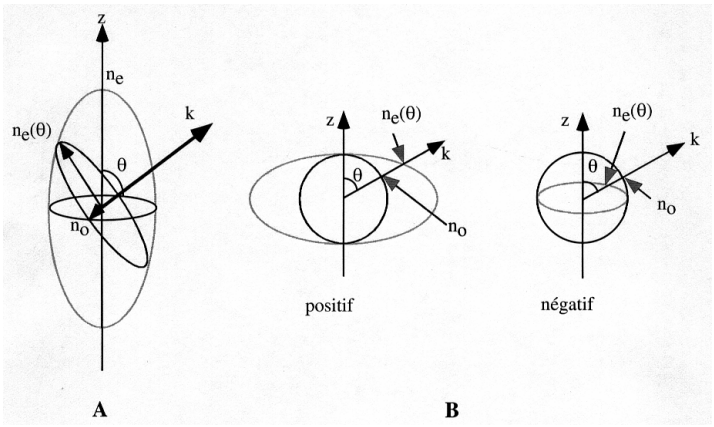

Figure 3.3: refractive index of an uniaxial crystal.

As shown by **Figure 3.3**, n_o is independent on the angle of propagation θ, while n_e is not. The function $n_o(\theta)$ is thus a circle, whereas $n_e(\theta)$ is an ellipse. **Figure 3.3 B** and **C** show these two functions for $n_o < n_e$ (positive crystal) and for $n_o > n_e$ (negative crystal). The magnitude of the axes depends on the frequency.

Figure 3.4 depicts n_o and n_e at ω_1 and at $2\omega_1$ for a negative crystal. This figure shows that there is an angle θ, where $n_o(\omega_1) = n_e(2\omega_1)$. At this angle, the phase matching condition for SHG is fulfilled. In this case, one speaks about type I phase matching, i.e. the polarisation of the new wave is perpendicular to that of the ω_1 wave.

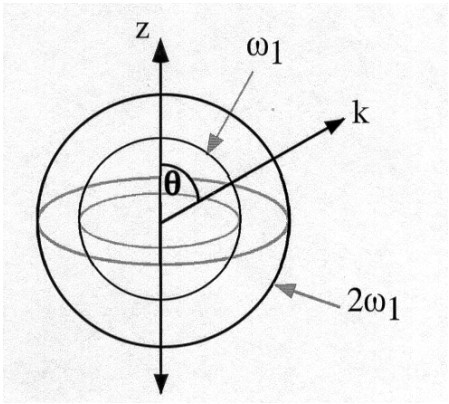

Figure 3.4: ordinary and extraordinary refractive indice of a negative uniaxial crystal at two frequencies.

For other processes like SFG, one can use either type I or type II phase matching. In the latter case, the waves at ω_1 and ω_2 are orthogonally polarised and the new wave at ω_3 has the same polarisation as one of the two incoming waves.
Temperature tuning of the crystal can also be used to find the condition $n_o(\omega_1) = n_e(2\omega_1)$.

4. Classical description of nonlinear susceptibility

The linear optical properties of a material can be described classically with the Lorentz model. In this case, the material is described as an ensemble of unidimensional damped harmonic oscillators of charge e and of mass m_e. Of course, a rigourous description of optical susceptibility requires a quantum mechanical treatment of matter, especially to account for all the transitions between the states of the molecules constituting the material. However, the Lorentz model is valid in the case where all the optical fields involved are at frequencies below that of the first electronic transition of the material.

The force exerted by an electric field on a charge e is :

$$F_E = -eE \tag{4.1}$$

In a neutral dielectric material, the charges are bound. There is therefore a restoring force F_R. The latter depends on the potential experienced by the charges. The variation of the potential energy V, as a function of the displacement of the charge from the equilibrium position, u, depends on the symmetry of the material.
For a material without a centre of inversion, it is given by :

$$V(u) = \frac{1}{2} m\omega_0^2 u^2 + \frac{1}{3} mau^3 \tag{4.2}$$

where m is the mass of the electron, ω_0 is the natural frequency, u the displacement out of the equilibrium position, and a is an anharmonicity parameter accounting for the nonlinear response of the material. With this potential, the restoring force is :

$$F_R = -\frac{dV}{du} = -m\omega_0^2 u - mau^2 \tag{4.3}$$

Newton's second law states that the sum of the forces acting on a body is equal to its mass mutiplied by its acceleration. Therefore, the equation of motion of the oscillator along u is :

$$\ddot{u} + 2\Gamma\dot{u} + \omega_0^2 u + au^2 = -eE(t)/m \tag{4.4}$$

where the second term on the l.h.s. accounts for the damping forces, Γ being a damping constant.

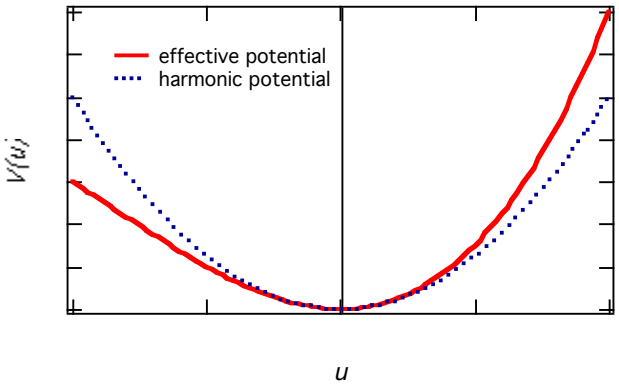

Figure 4.1: potential for a non-centrosymmetric material.

The electric field will be expressed as :

$$E(t) = E_1 \exp(-\omega_1 t) + E_1 \exp(-\omega_2 t) + c.c. \tag{4.5}$$

Equation (4.4) is solved using the perturbation technique. To do this, one replace $E(t)$ in (4.4) by $\varsigma E(t)$, where ς is a perturbation parameter :

$$\ddot{u} + 2\Gamma\dot{u} + \omega_0^2 u + au^2 = -e\varsigma E(t)/m \tag{4.6}$$

The displacement $u(t)$ is then expanded in a power series of ς :

$$u = \varsigma u^{(1)} + \varsigma^2 u^{(2)} + \varsigma^3 u^{(3)} + ... \tag{4.7}$$

Equation (4.7) is then inserted into equation (4.6). The resulting terms are then sorted according to their power dependence on ς. If we stop at the third order, we obtain three equations that have to be satisfied simultaneously :

$$\ddot{u}^{(1)} + 2\Gamma\dot{u}^{(1)} + \omega_0^2 u^{(1)} = -eE(t)/m \tag{4.8a}$$

$$\ddot{u}^{(2)} + 2\Gamma\dot{u}^{(2)} + \omega_0^2 u^{(2)} + a\left(u^{(1)}\right)^2 = 0 \tag{4.8b}$$

$$\ddot{u}^{(3)} + 2\Gamma\dot{u}^{(3)} + \omega_0^2 u^{(3)} + 2au^{(1)}u^{(2)} = 0 \tag{4.8c}$$

Equation (4.8a) is identical to the equation of motion of an damped harmonic oscillator (Lorentz model).

$$u^{(1)}(t) = u^{(1)}(\omega_1)\exp(-i\omega_1 t) + u^{(1)}(\omega_2)\exp(-i\omega_2 t) + c.c. \tag{4.9}$$

with the amplitudes :

$$u^{(1)}(\omega_j) = -\frac{e}{m}\frac{E_j}{\omega_0^2 - \omega_j^2 - 2i\omega_j\Gamma} = -\frac{e}{m}\frac{E_j}{\mathrm{D}(\omega_j)} \tag{4.10}$$

This result is then used to solve equation (4.8b). The square of (4.9) contains terms oscillating at frequencies $\pm 2\omega_1$, $\pm 2\omega_2$, $\pm(\omega_1-\omega_2)$, $\pm(\omega_1+\omega_2)$ and 0.

For example, the response at frequency $2\omega_1$ can be found by solving the following equation :

$$\ddot{u}^{(2)} + 2\Gamma\dot{u}^{(2)} + \omega_0^2 u^{(2)} = -\frac{a(eE_1/m)^2\exp(-i2\omega_1 t)}{\mathrm{D}^2(\omega_1)} \tag{4.11}$$

To solve (4.11), the following trial solution is inserted :

$$u^{(2)}(t) = u^{(2)}(2\omega_1)\exp(-2\omega_1 t) \tag{4.12}$$

One obtains for the amplitude :

$$u^{(2)}(2\omega_1) = -\frac{a(e/m)^2 E_1^2}{\mathrm{D}(2\omega_1)\mathrm{D}(\omega_1)\mathrm{D}(\omega_1)} \tag{4.13}$$

The same procedure can be used to obtain the amplitudes at the other frequencies.

The product eu is a dipole moment. Because $u(t)$ oscillates with a $2\omega_1$ frequency component, the polarisation exhibits such a component as well :

$$P^{(2)}(2\omega_1) = Neu^{(2)}(2\omega_1) \tag{4.14}$$

This component of the nonlinear polarisation is related to the nonlinear susceptibility as follows :

$$P^{(2)}(2\omega_1) = \varepsilon_0 \chi^{(2)}(2\omega_1, \omega_1, \omega_1) E(\omega_1)^2 \tag{4.15}$$

Using equation (4.13) one obtains :

$$\chi^{(2)}(2\omega_1, \omega_1, \omega_1) = -\frac{Nae^3/\varepsilon_0 m^2}{\mathrm{D}(2\omega_1)\mathrm{D}(\omega_1)\mathrm{D}(\omega_1)} \tag{4.16}$$

$\chi^{(2)}(2\omega_1, \omega_1, \omega_1)$ is a complex quantity. It can be splitted into a real and an imaginary parts :

$$\chi^{(2)} = \chi_r^{(2)} + i\chi_i^{(2)} \tag{4.17}$$

Figure 4.2 shows the spectrum of $\chi^{(2)}(2\omega_1, \omega_1, \omega_1)$ as well as that of $\left|\chi^{(2)}(2\omega_1, \omega_1, \omega_1)\right|^2$, which corresponds to the frequency dependence of the SHG intensity. One can see that

the SHG efficiency is larger near ω_0, i.e. in resonant conditions. This frequency also corresponds to a resonance of $\chi^{(1)}$ and therefore the material will absorb there.

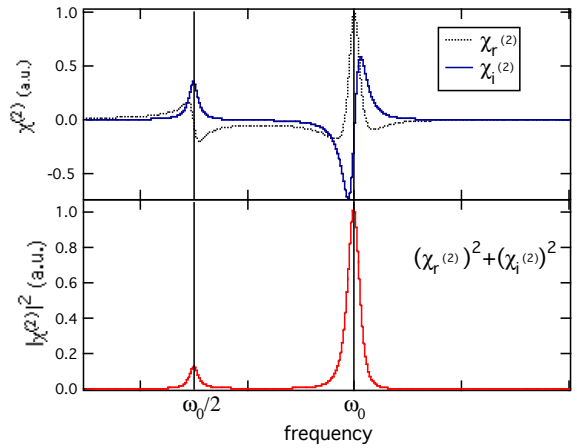

Figure 4.2: frequency dependence of the real and imaginary parts of $c^{(2)}$ and of $|c^{(2)}|^2$ calculated using (4.16).

One can also see that $\chi^{(2)}(2\omega_1, \omega_1, \omega_1)$ has a resonance at $\omega_0/2$. This corresponds to a resonance for a two-photon absorption. In general, these absorption problems are avoided by performing SHG at frequencies far from these resonances. This of course leads to a reduced SHG efficiency.

For material with a centre of inversion, the potential $V(u)$ is different from (4.2) and is symmetric for the inversion ($V(-u)=V(u)$). Its shape is thus similar to that shown in **Figure 4.3**. The restoring force, F_R, is not a u^2 term (see (4.3)) but a u^3 term. Therefore the equation of motion is different.

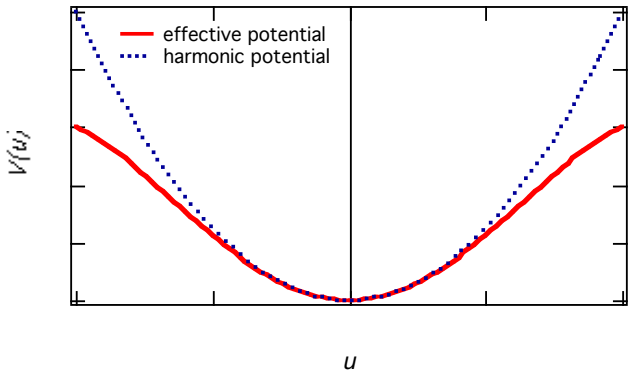

Figure 4.3: potential for a centrosymmetric material.

An important consequence of the symmetry is that the nonlinear susceptibility tensors of even orders vanish for such centrosymmetric materials.

One can see this by the perturbation treatment used above (see equation (4.4)) with non-centrosymmetric materials, to obtain the equation equivalent to (4.8b):

$$\ddot{u}^{(2)} + 2\Gamma\dot{u}^{(2)} + \omega_0^2 u^{(2)} = 0 \qquad (4.18)$$

This equation is the equation of motion of a damped oscillator without a driving force. Its steady state solution is $u^{(2)} = 0$.

The absence of even order nonlinearity of centrosymmetric material can also be understood by considering even order polarisation :

$$P^{(2n)} = \chi^{(2n)} \cdot E^{2n} \qquad \text{n=1,2,3…} \qquad (4.19)$$

In a centrosymmetric material, an inversion of the sign of the electric field results in an inversion of the polarisation :

$$-P^{(2n)} = \chi^{(2n)}(-E)^{2n} = \chi^{(2n)}E^{2n} \qquad (4.20)$$

By comparing (4.20) with (4.19), one can see that $-P^{(2n)} = P^{(2n)}$, which is only possible if $\chi^{(2n)} = 0$. Consequently, material with a centre of inversion do not show any even order nonlinear response ! This concerns of course materials consisting of molecules with a centre of inversion, but also centrosymmetric materials on a macroscopic point of view. Isotropic materials, like liquids and glasses, have thus no even order nonlinear optical property. For such materials, the first nonlinear contribution originates from the third order susceptibility.

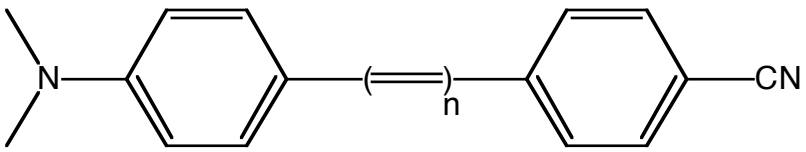

Figure 4.4: push-pull molecule with second order nonlinear optical properties.

The most widely used second order nonlinear materials are inorganic crystals like KDP (KH_2PO_4), BBO (b-BaB_2O_4), and LBO (LiB_3O_5). The number of non vanishing tensor elements of $\underline{\chi}^{(2)}$ depends on the symmetry of the crystal.

Many research groups are trying to synthetise organic materials with second order nonlinear properties.

If one calculates the nonlinear susceptibility using a quantum description of matter, one obtains the following expression for the second order hyperpolarisability :

$$\beta(\omega) \approx \frac{3he^2}{2m} \frac{\omega_{ba} f \Delta\mu}{\left(\omega_{ba}^2 - \omega^2\right)^2 \left(\omega_{ba}^2 - 4\omega^2\right)} \qquad (4.21)$$

where ω_{ba} is the angular frequency associated to the transition between the states |a> and |b>, f is the oscillator strength of this transition and $\Delta\mu$ is the difference of permanent dipole moment between |a> and |b>. Molecules with electronic transitions involving a strong charge transfer are therefore the best candidates for second order nonlinear materials. These are push-pull type molecules containing electron donating and accepting groups as that illustrated in **Figure 4.4.** In order to be active, the material has to be macroscopically noncentrosymmetric. For this, these molecules have to be specifically oriented.

5. Some applications of second order nonlinear processes

Optical parametric oscillators and amplifiers

We have already mentionned frequency conversion processes that allow the generation of new frequencies from a laser source. If the laser is monochromatic and not tunable, SHG will also give monochromatic light.

However, optical parametric oscillations (OPO) allow the generation of coherent and tunable radiation. The basic principle is parametric fluorescence. If a material with a $\chi^{(2)} \neq 0$ is irradiated with an intense radiation at ω_3, new radiation at ω_1 and ω_2 will be spontaneously emitted. The relationship between these radiations is :

$$\omega_1 + \omega_2 = \omega_3 \qquad (5.1)$$

Of course, the phase matching condition has to be fulfilled :

$$\vec{k}_1 + \vec{k}_2 = \vec{k}_3 \qquad (5.2)$$

Several ω_1/ω_2 pairs satisfiy (5.1) and (5.2) and thus the light is emitted a cone with concentric circles of different colours.

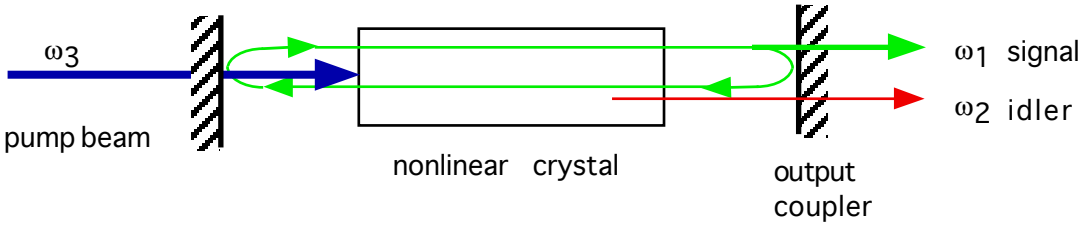

Figure 5.1: schematic layout of an OPO

An OPO consists in such a nonlinear material inserted in an optical cavity, allowing the feedback of parametric fluorescence in the material, and thus its amplification (see **Figure 5.1**). If gain exceeds losses, oscillation takes place. Only the ω_1/ω_2 pair that propagates exactly along the cavity axis can undergo amplification. If the mirrors have the same reflectivity at ω_1 and ω_2, the oscillator is doubly resonant, such an OPO generates coherent light at both ω_1 and ω_2.

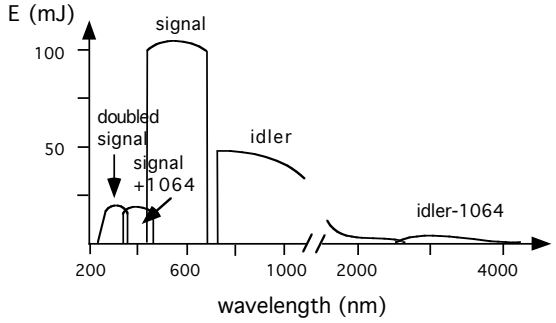

Figure 5.2: typical output of an OPO pumped by 420 mJ pulses at 355 nm generated by a Q-switched Nd :YAG laser.

Frequency tuning can be achieved by varying the phase matching condition, either by varying the angle of the crystal or by changing its temperature. By convention, the high frequency beam is called *signal*, while the low frequency beam is called *idler*. If one pumps such an OPO at 355 nm, it is possible to generate coherent light tunable between 400 and 3000 nm (see **Figure 5.2**).

The optical parametric amplifier (OPA) is another a device based on parametric fluorescence. An OPA amplifies a weak intensity beam at ω_1. This beam travels through a nonlinear material while pumped by an intense beam at ω_3. Contrarily to a conventional amplifier, parametric amplification requires the temporal coincidence of the beams (pulses) at ω_1 and ω_3.

Fluorescence up-conversion

The up-conversion technique is based on SFG. It enables the conversion of a weak signal at ω_1 to a signal at at ω_3 upon interaction with an intense light beam at ω_2, with $\omega_3 = \omega_1 + \omega_2$. Historically, this technique has been mainly used to convert weak IR signals into visible signals, where light detectors are more sensitive and cheaper.

This technique is also used in ultrafast spectroscopy to measure fluorescence dynamics on timescales shorter than one nanosecond.

The principle of this pump-probe technique is illustrated in **Figure 5.3**. An ultrashort laser pulse at ω_1 is first focused on a nonlinear crystal for SHG. The pulse at $2\omega_1$ is used to excite the sample (pump pulse). The unconverted pulse at ω_1, the probe (or gate) pulse, is sent on a movable retroreflector before being focused on a nonlinear crystal for SFG. The fluorescence at ω_F, generated by the sample excited at $2\omega_1$, is also focused onto this crystal. In this crystal, light at ω_F and the pulse at ω_1 temporally overlap during the duration of the gate pulse. Due to SFG, a weak pulse, the signal, at $\omega_S = \omega_F + \omega_1$ is generated (see **Figure 5.4**). The signal intensity is proportional to the fluorescence intensity at the time where it interacts with the probe/gate pulse. If this pulse arrives on the crystal at the same time as the fluorescence maximum, a strong ω_s signal is generated.

If however, the gate pulse arrives on the crystal much later than the lifetime of the fluorescence, a weak ω_S signal is generated.

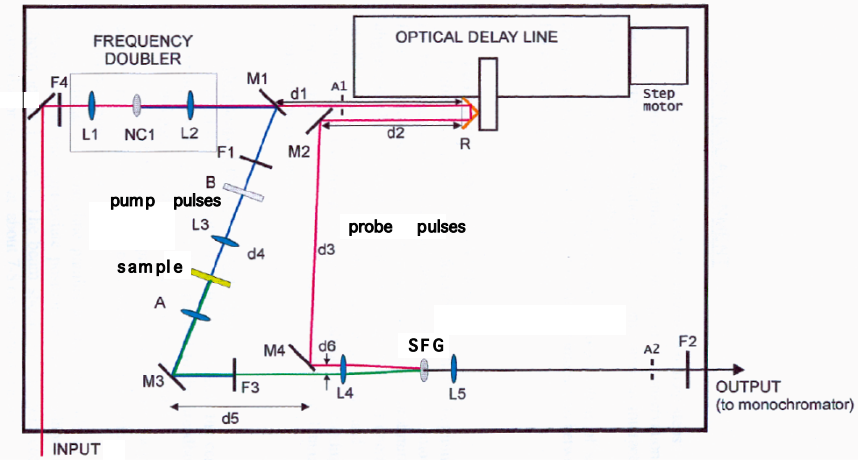

Figure 5.3: time-resolved fluorescence up-conversion setup.

Thus, the technique consists in measuring the ω_S signal as a function of the arrival time of the gate pulse on the crystal relatively to the beginning of the fluorescence. For this, the optical path of the gate pulse has to be lengthened relatively to that of the fluorescence. A pathlength difference of 1 mm corresponds to a time delay of 3.3 ps.

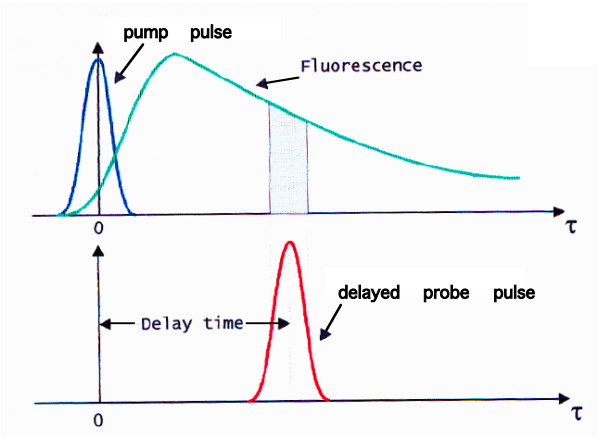

Figure 5.4: principle of fluorescence up-conversion.

After the crystal, light contains ω_F, ω_I and ω_S. The components of ω_F, and ω_I are filtered out with a monochromator located in front of the detector.

Figure 5.5 shows the time profile of the fluorescence emitted by the S_2 state of a porphyrin, measured by this technique. The temporal resolution depends mainly on the duration of the laser pulses. For a temporal resolution better than 100 fs, other parameters, such as the geometry and the group velocity dispersion, have to be taken into account.

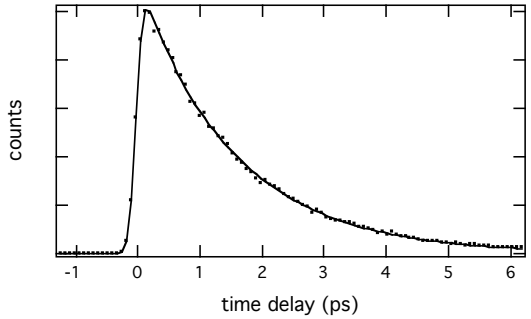

Figure 5.5: S_2 fluorescence dynamics of a porphyrin in toluene.

Surface-SHG and SFG

The absence of second order nonlinear response of centrosymmetric materials can be used to study selectively the interface between two isotropic materials. Indeed, such an interface is no longer centrosymmetric and therefore has a nonvanishing second order nonlinear response.

For example, let's consider an isotropic liquid in contact with air. If one irradiates this interface with an intense beam at ω_1 and if one detects a signal at $2\omega_1$, one can be sure that this signal originates exclusively from the air/liquid interface.

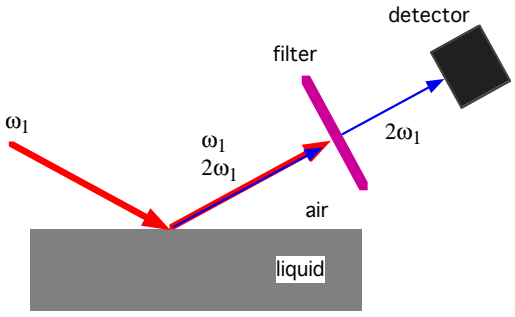

Figure 5.6: principle of surface SHG of an air/liquid interface.

This selectivity of SHG (or also of SFG) makes it a very valuable spectroscopic tool for the study of interfaces and surfaces.

We will illustrate this technique with two examples. **Figure 5.6** shows the principle of SHG at an air/liquid interface. One uses a pulsed laser in order to obtain a high light intensity and also, in some cases, to have dynamic information. From **Figure 3.2**, one can see that the SHG efficiency increases as the frequency approach the resonance frequency. In fact, if one measures the SHG intensity as a function of the frequency, one obtains a spectrum that reflects the absorption spectrum of the material. This property has been used to characterise the polarity of an air/liquid interface.

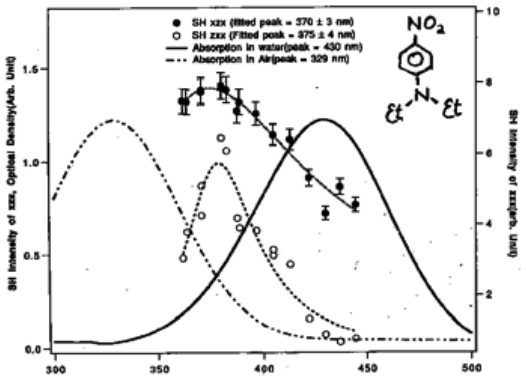

Figure 5.7: SHG spectrum of nitroaniline at the air/water interface and absorption spectra in the gas phase and in water (from K. B. Eisenthal, Lecture Notes, Champery 2000).

Figure 5.7 shows the SHG intensity of para-nitroaniline at the air/water interface and its absorption spectrum in water and in the gas phase. One can see that the interfacial polarity is the average of the polarity of water and air. Similar observations were made at liquid/liquid interfaces. The interpretation is that at the interface, the molecule is half in the solvent, half in air.

One can also perform pump-probe time-resolved SHG measurements. One uses a first pulse to excite the molecules at the interface, and a second pulse at a frequency one-photon or two-photon resonant with the molecule to perform SHG. **Figure 5.8** depicts the time profile of the SHG intensity at 400 nm measured with malachite green (MG) in water at the interface with dodecane upon excitation at 600 nm. The signal at 400 nm is resonant with the S_2<-S_0 transition and thus the intensity reflects the recovery of the ground-state population. The excited-state lifetime of MG depends strongly on the viscosity of the environment because torsion of the phenyl rings leads to a S_1/S_2 conical

intersection, hence to non-radiative deactivation of the excited state. Therefore, the lifetime of MG S_1 state can be used as a local probe of viscosity. The excited-state lifetime of MG at the dodecane/water interface is around 2 ps, whereas it is only 500 fs in bulk water. Thus, the friction exerted by interfacial water is much larger than that exerted by bulk water.

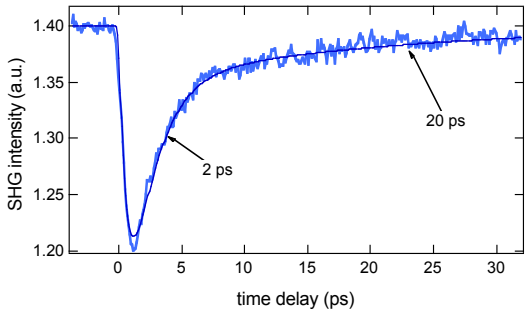

Figure 5.8: time-profile of the SHG intensity at 400 nm measured with Malachite Green in water at the interface with dodecane after 600 nm excitation.

6. Third order nonlinear optical susceptibility

The mathematical expression for $\chi^{(3)}$ obtained from the time dependent perturbation theory can be expressed as the sum of 48 terms of this type:

$$\chi^{(3)}_{kijh}\left(\omega_p+\omega_q+\omega_r,\omega_r,\omega_q,\omega_p\right)\propto \frac{\mu^k_{lv}\mu^j_{vn}\mu^i_{nm}\mu^h_{ml}}{\left[\left(\omega_{vl}-\omega_p-\omega_q-\omega_r\right)-i\Gamma_{vl}\right]\left[\left(\omega_{nl}-\omega_p-\omega_q\right)-i\Gamma_{nl}\right]\left[\left(\omega_{ml}-\omega_p\right)-i\Gamma_{ml}\right]}+\ldots \quad (6.1)$$

where μ is a transition dipole and where the signification of the various indices is illustrated in **Figure 6.1**. One can thus see that there are many possibilities for resonances. As there are 81 tensor elements of $\chi^{(3)}$, one can imagine the richness and complexity of this tensor.

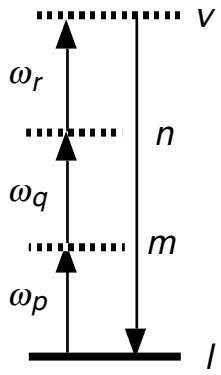

Figure 6.1: energy level scheme related to equation (6.1).

We will mainly consider isotropic materials. Due to their symmetry, the $\chi^{(3)}$ tensor contains only 21 non vanishing elements :

$$\begin{aligned}
&\chi^{(3)}_{1111}=\chi^{(3)}_{2222}=\chi^{(3)}_{3333}\\
&\chi^{(3)}_{1122}=\chi^{(3)}_{1133}=\chi^{(3)}_{2211}=\chi^{(3)}_{2233}=\chi^{(3)}_{3311}=\chi^{(3)}_{3322}\\
&\chi^{(3)}_{1212}=\chi^{(3)}_{1313}=\chi^{(3)}_{2323}=\chi^{(3)}_{2121}=\chi^{(3)}_{3121}=\chi^{(3)}_{3232}\\
&\chi^{(3)}_{1221}=\chi^{(3)}_{1331}=\chi^{(3)}_{2112}=\chi^{(3)}_{2332}=\chi^{(3)}_{3113}=\chi^{(3)}_{3223}
\end{aligned} \quad (6.2)$$

where the indices 1,2,3 design the cartesian coordinates. For example, the element $\chi^{(3)}_{1111}$ is responsible for the 1 component (*x*, *y*, or *z*) of the polarisation, due to the 1 component

of each of the three applied electric fields. Experimentally, if one crosses three light beams polarised along the same direction on an isotropic material, the generated signal field is also polarised along this polarisation. This beam geometry measures only $\chi^{(3)}_{1111} = \chi^{(3)}_{2222} = \chi^{(3)}_{3333}$.

Moreover, the four classes of tensor elements in (6.2) are not independent and are related as follows :

$$\chi^{(3)}_{1111} = \chi^{(3)}_{1122} + \chi^{(3)}_{1212} + \chi^{(3)}_{1221} \qquad (6.3)$$

Depending on the details of the experiment that is performed, the number of independent elements can be even smaller. For example, in the third harmonic generation, the three applied fields are at the same frequency and their permutation gives the same result. In this case, $\chi^{(3)}_{1212} = \chi^{(3)}_{1221} = \chi^{(3)}_{1122}$.

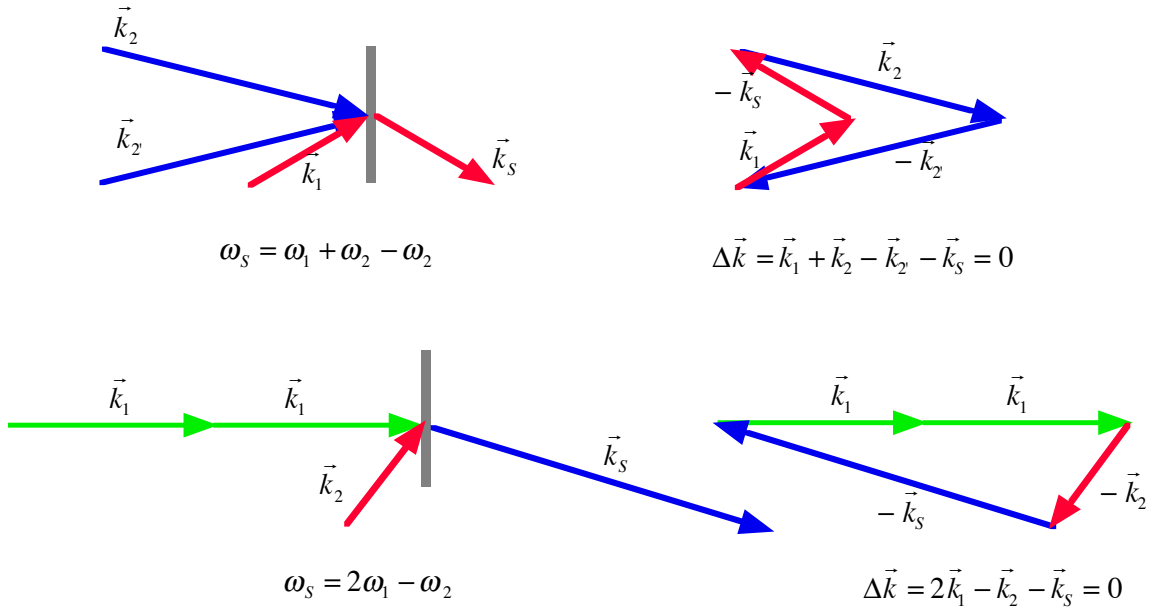

Figure 6.2: beam arrangements satisfying the phase matching condition for transient grating (top) and for CARS (bottom).

If one considers a radiation field containing three frequencies, ω_1, ω_2 and ω_3, interacting with a material, one can see that the third order polarisation, $P^{(3)}$, contains the following combination of frequencies :

$$\omega_1 + \omega_2 + \omega_3 \tag{6.4a}$$

$$3\omega_j,\ \omega_j \qquad j=1,2,3 \tag{6.4b}$$

$$2\omega_i + \omega_j,\ 2\omega_i - \omega_j,\ \omega_i - 2\omega_j \qquad i=1,2,3,\ j\neq i; \tag{6.4c}$$

$$\omega_i + \omega_j - \omega_k,\ \omega_i - \omega_j - \omega_k \qquad i=1,2,3,\ k\neq j\neq i \tag{6.4d}$$

A beam at a given frequency is of course only generated if the phase matching condition is satisfied. In an isotropic material, this condition cannot be fulfilled for processes where the signal is at the sum frequency of the three applied beams (for example, $\omega_1 + \omega_2 + \omega_3$, $3\omega_j$ and $2\omega_i + \omega_j$).

For the other processes, the phase matching condition can be satisfied by adjusting the angle of incidence of the various beams, as shown in **Figure 6.2**.

7. Self-induced nonlinear processes

By self-induced process, one designs a process where the properties of a light beam are modified by the beam itself. The most common self-induced phenomena are due to the nonlinear refractive index.

At high light intensity, the refractive index, n, of the material can be written as :

$$n = n_0 + 2\bar{n}_2 \left|E_0\right|^2 \tag{7.1}$$

where n_0 is the linear refractive index (see equation (1.10)), E_0 is the electric field amplitude (see equation 3.4-5) and $\bar{n}_2$ is the second order nonlinear refractive index.

This nonlinear refractive index is easily understood if one considers that the propagation of an intense light beam in a material is accompanied by the orientation of the electric charges along the associated electric field. The polarisation of the electrons is quasi-instantaneous and follows the oscillations of the electric field even at optical frequencies.

If the molecules have a permanent or an induced dipole moment, they reorient along the field. However, this motion is too slow relatively to the oscillation of the optical field. There are however, components of the field at $\omega = 0$ (optical rectification), that can induce molecular reorientation. After this electronic and nuclear reorientation, the material is no longer isotropic and therefore the refractive index along the optical electric field is not the same as that in the other directions. This difference increases with $|E_0|^2$, i.e.with the light intensity *I*. This photoinduced birefringence is called *Optical Kerr Effect* (OKE).

The nonlinear polarisation responsible for this effect is :

$$P^{(3)}(\omega) = 3\varepsilon_0 \chi^{(3)}(\omega = \omega + \omega - \omega)|E(\omega)|^2 E(\omega) \qquad (7.2)$$

One can show that the nonlinear refractive index is related to $\chi^{(3)}$ as follows :

$$\bar{n}_2 = \frac{3\chi^{(3)}}{4n_0} \qquad (7.3)$$

Similarly to $\chi^{(3)}$, the nonlinear refractive index is a fourth rank tensor. It is often expressed as :

$$n = n_0 + n_2 I \qquad (7.4)$$

with

$$n_2 = \frac{(\mu_0/\varepsilon_0)^{1/2}}{2n_0}\bar{n}_2 \qquad (7.5)$$

The value of n_2 (for the 1111 geometry) of several materials, is listed below.

Material	n_2 (cm^2/W)	response time
Air (20ºC)	$4.7\text{x}10^{-19}$	
CS_2	$1.7\text{x}10^{-13}$	2 ps
Optical glass	$1\text{-}100\text{x}10^{-16}$	ultrafast
Polydiacetylene	$4.5\text{x}10^{-12}$	ultrafast

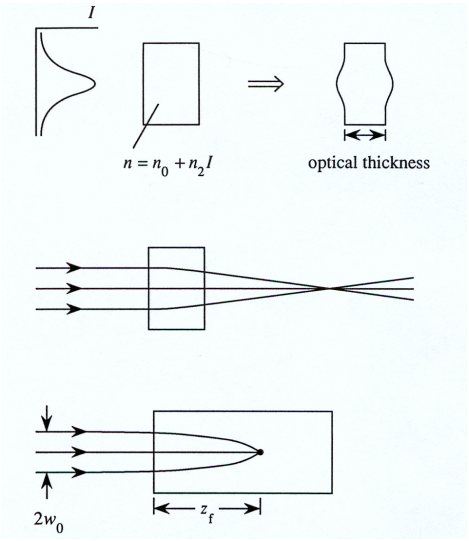

Figure 7.1: self-focussing.

This table shows that the optical Kerr effect induces an increase of refractive index.

In general, the spatial distribution of the light intensity of a laser is gaussian. If such a beam propagates in a material with a non zero n_2, it induces a similar spatial distribution of the refractive index, with a large refractive index in the centre than on the edges.

As a consequence, the material becomes a positive lens, that focuses the beam (see **Figure 7.1**). This effect is called self-focussing. If the material is long, the focus can be located inside. This can induce irreversible damages in the material. This phenomenon has always to be accounted for when designing the cavity of a pulsed laser.

If the light is pulsed, the refractive index of the material is time dependent :

$$n(t) = n_0 + n_2 I(t) \tag{7.6}$$

The electric field associated to a laser pulse can be described by :

$$E(z,t) = A(t) \cdot \exp\left[i\left(kz - \omega_0 t + \phi\right)\right] \tag{7.7}$$

where $A(t)$ is the pulse envelope ϕ is the phase acquired by the wave propagating in a material of refractive index over a length L:

$$\phi = -\frac{n\omega_0 L}{c} \tag{7.8}$$

If the pulse is intense, n should be described as in (7.6) and thus the phase is time dependent :

$$\phi^{NL} = -\frac{n_2 I(t)\omega_0 L}{c} \tag{7.9}$$

with $$I(t) = 2n_0\left(\varepsilon_0/\mu_0\right)^{1/2}\left|A(t)\right|^2 = I_0\,\mathrm{sech}^2\left[\frac{t}{0.568\cdot\tau_p}\right] \tag{7.10}$$

where τ_p is the duration of the pulse (full width at half maximum).

The electric field at the output of the material is obtained by inserting (7.10) in (7.9) and then in (7.7). **Figure 7.2** shows the electric field calculated for a 15 fs pulse with an overexagerated value of n_2.

This figure shows that the instantaneous frequency varies continuously : the frequencies at the leading edge of the pulse are shifted to the red, while those at the trailing edge are blue shifted. This is due to the fact that the temporal variation of the phase corresponds to a frequency variation.The instantaneous frequency variation is :

$$\delta\omega(t) = \frac{\partial\phi^{NL}(t)}{\partial t} = \frac{2n_2\omega_0 L}{c} I_0\,\mathrm{sech}^2\left(\frac{t}{0.568\tau_p}\right)\tan\left(\frac{t}{0.568\,\tau_p}\right) \tag{7.11}$$

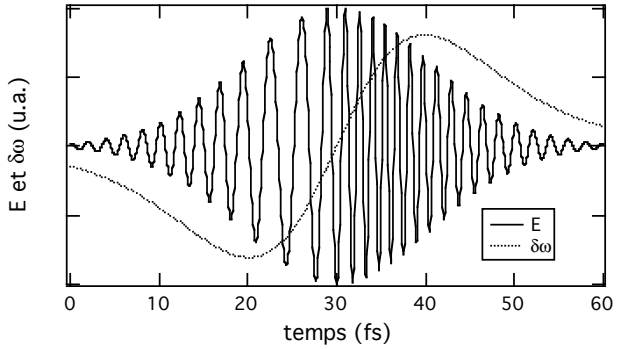

Figure 7.2: electric field associated to a 15 fs pulse after self-phase modulation and variation of the instantaneous frequency (the effect has been exagerated).

This variation of frequency is illustrated in **Figure 7.2**. This phenomenon is called *self-phase modulation* and is used to broaden the spectrum of a laser pulse. One obtains in this way a continuous spectrum extending over all the visible region. As an example, **Figure 7.3** shows the spectral continuum obtained upon focussing 25 ps laser pulses at 1064 nm in a D_2O/H_2O mixture. In principle, this process is observed in all materials (even in air).

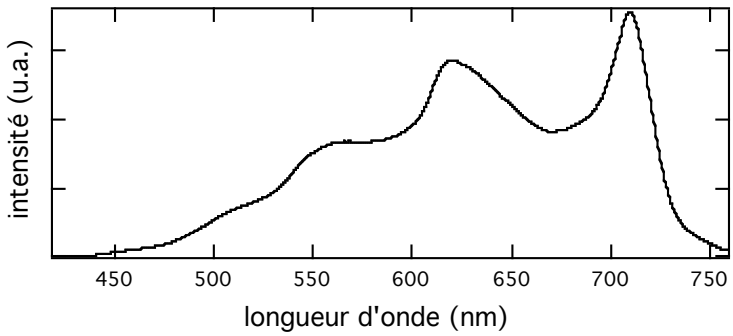

Figure 7.3: spectrum of the white light continuum obtained by focussing a 25 ps pulse at 1064 nm in a D_2O/H_2O mixture.

The optical Kerr effect is a non-resonant process due to the real part of the third order nonlinear susceptibility hence of the third order polarisation, $P^{(3)}$. Howerer, $\chi^{(3)}$, has many resonances and one of them occurs when the incoming field is at half a transition frequency of the material, $\omega = \omega_{ba}/2$ (**Figure 7.4**). In this case, the polarisation oscillates at $\omega_{ba}/2$, and as it possess an imaginary component, it can exchange energy with the optical field. This results to absorption of light at $\omega_{ba}/2$. Overall, two $\omega_{ba}/2$ photons are absorbed in this process, which is thus called *two-photon absorption* (TPA). Contrary to the intuition, TPA is not a second-order process but a third order phenomenon. The phase matching conditions are automatically fulfilled as no new frequency is generated.

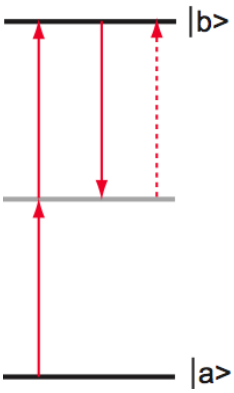

Figure 7.4: energy level scheme for TPA. Three field interaction generate a third order polarisation. Further interaction with the optical field result the net absorption of two photons.

With the development of compact femtosecond lasers, there is presently a strong interest for molecules exhibiting intense TPA. One application is two-photon excited fluorescence, where the fluorescence from a molecule is detected upon TPA. One advantage over one photon absorption (OPA) is that, because the TPA probabilitly

depends on the square of the excitation intensity, the fluorescence is predominantly emitted from the focal region of the excitation beam, allowing superior spatial resolution for fluorescence imaging. For medical applications, TPA is also advantageous, because light at long wavelengths is less absorbed and less scattered by living tissues. Thus, exciting a photosensitiser or a fluorescence probe by TPA instead of OPA allows a better penetration depth.

The superior spatial resolution of TPA is also used in two-photon induced photopolymerisation (TPIP) to realise very precise microstructures (**Figure 7.5**).

Because of the conservation of momentum, OPA is only possible between states of different parity. For the same reason, TPA is only possible between state having the same parity. Thus optical transitions that are not visible by OPA may be intense in the TPA spectrum. This difference become less important are the symmetry of the molecule decreases.

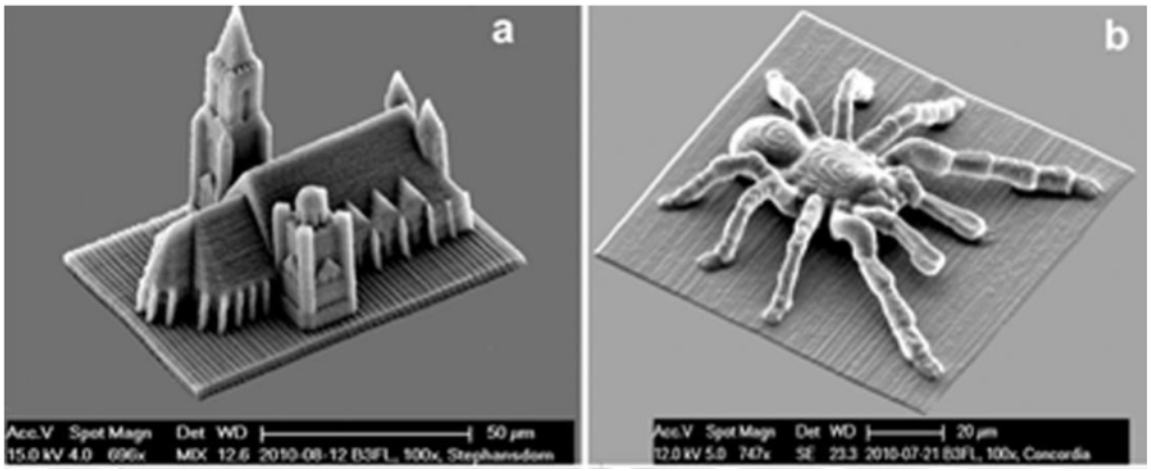

Figure 7.5: 3D structures realised by two-photon initiated photopolymerisation (from Z. Li et al., *J. Polym. Sci. A 49,* **2011**, 3688-99)

8. Some spectroscopic applications related to $\chi^{(3)}$

Time-resolved optical Kerr effect

As mentionned above, the optical Kerr effect is a birefringence due to the electronic and nuclear polarisation under the influence of light. The electronic response is essentially instantaneous, while the nuclear polarisation involves molecular reorientation. Once the electric field is stopped, the electronic birefringence ceases immediately, while the decay of the nuclear birefringence requires molecular reorientation as well. Consequently, the measurement of the temporal variation of the nuclear birefringence gives information on the dynamics of liquids.

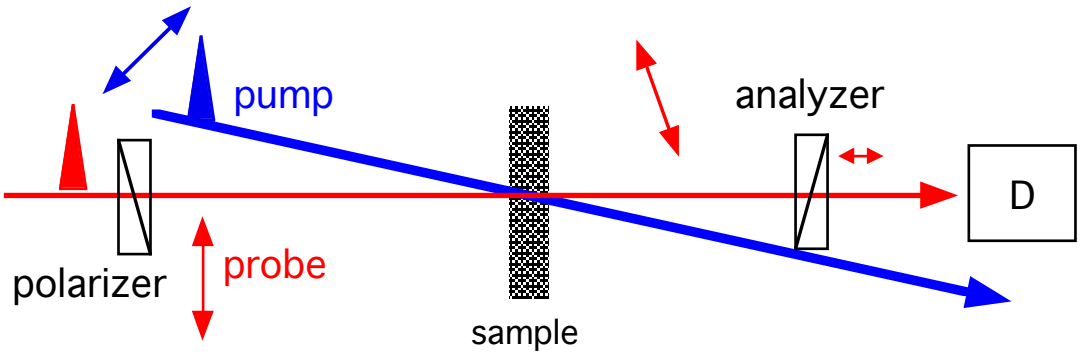

Figure 8.1: principle of measurement of the time-dependent OKE.

An experimental setup for measuring the dynamics of the optical Kerr effect is shown in **Figure 8.1**.

The sample is located between two crossed polarisers. Therefore, the probe pulses cannot reach the detector. At time $t=0$, the sample is illuminated by a pump pulse linearly polarised at 45^0 relatively to the first polariser (see **Figure 8.2**). This pump pulse creates a birefringence, the refractive index parallel to the polarisation, $n_{\parallel}$, being larger than that perpendicular to it, $n_{\perp}$.

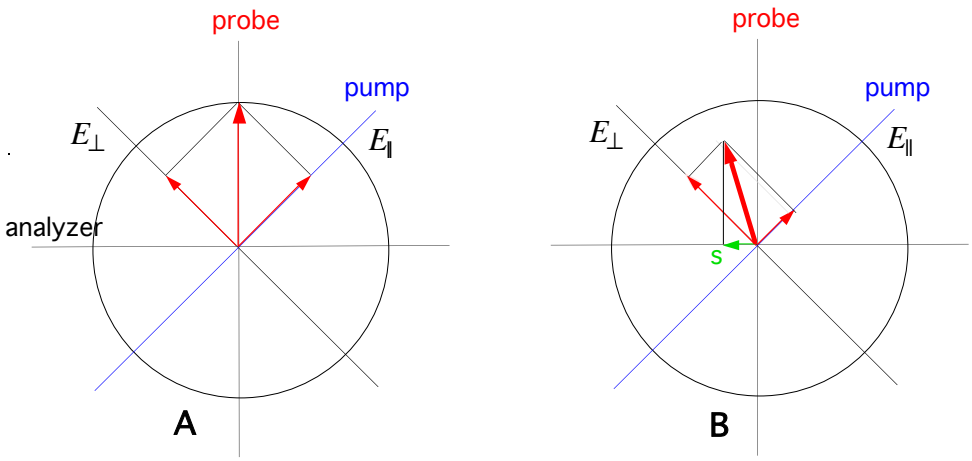

Figure 8.2: principles of the OKE measurement. If there is no birefringence (**A**), the probe pulse is blocked by the analyser. With birefringence (**B**), the polarisation of the probe pulse is slightly rotated and its component parallel to the analyser can travel through it.

The electric field associated to the probe pulse can be decomposed into two components : parallel $E_\parallel$, and perpendicular $E_\perp$ to the polarisation of the pump pulse. At the entrance of the sample, these two components are in phase, $\Delta\phi = 0$ (A). In the birefringent sample, each component feels a different refractive index ($n_\parallel$ or $n_\perp$) and thus propagates at a different phase velocity. At the output, these components are dephased, $\Delta\phi \neq 0$, and if we add them, one can see that the polarisation of the resulting total field has undergone a rotation (B in **Figure 8.2**). This total field has now a component parallel to the analyser (S) which can cross it and reach the detector.

The dephasing due to birefringence is :

$$\Delta\phi = \frac{\omega}{c}(n_\parallel - n_\perp)L \qquad (8.1)$$

where L is the optical pathlength in the sample. The light intensity transmitted by the analyser is :

$$I_T \propto \sin^2\left(\frac{\Delta\phi}{2}\right) \qquad (8.2)$$

One can show that this intensity is proportional to the following tensor elements :

$$I_T \propto \left|\chi^{(3)}_{1122} + \chi^{(3)}_{1221}\right|^2 \qquad (8.3)$$

Figure 8.3 shows the time profile of I_T measured in toluene.

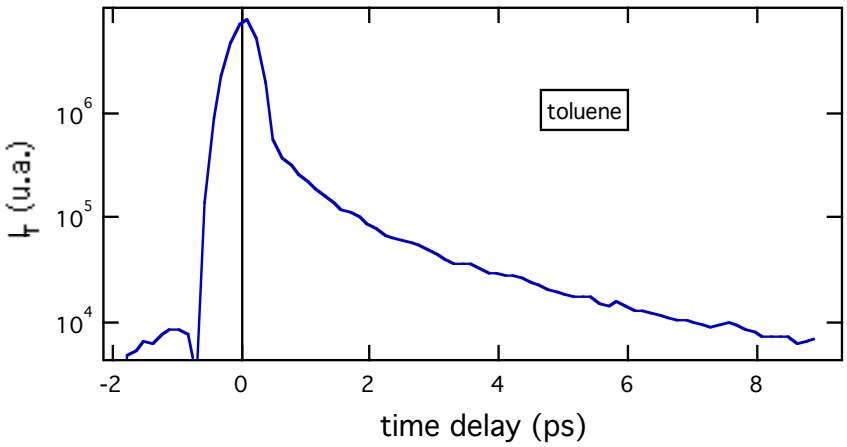

Figure 8.3: OKE measurement in toluene (pump : 400nm, probe : 690 nm).

The peak at *t=0* is due to the electronic response of the solvent and the slow component reflects the molecular reorientation of toluene (nuclear response). This reorientation dynamics is complexe and involves time constants of the order of 500 fs and 2-3 ps.

RIKES (Raman Induced Kerr Effect Spectroscopy)

If one considers equation (6.1), one can see that, depending on the frequency of the light beams, for example $\omega_p + \omega_q + \omega_r = \omega_{vl}$, the denominator becomes very small and the optical susceptibility becomes very large. This means that the energies of the photons involved coincide with a transition between stationary states of the material. This effect is called resonance enhancement. **Figure 8.4A** shows an energy level scheme similar to that of **Figure 6.1** but for OKE as described in the previous section. In this case, there is no resonance.

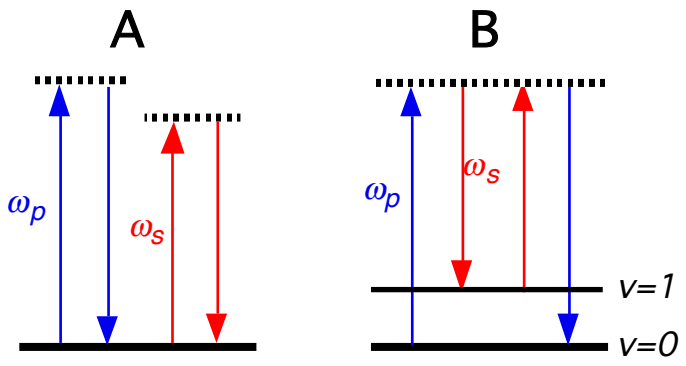

Figure 8.4: schematic representation of the non resonant OKE (A) and of the RIKES (B).

However, if the frequency difference of the pump and probe beams is equal to a vibrational frequency of a Raman active mode of the molecule, one obtains the situation depicted in **Figure 8.4B**. In this case, there is resonance and thus enhancement of the Kerr effect. This effect is used in RIKES where one measures the birefringence as a function of the frequency difference between the pump and probe pulses.

Pratically, one of the beams is at constant frequency, while that of the other beam is scanned. The time delay between the pump and probe pulses has to be essentially zero (in fact, inferior to the vibrational dephasing time).

The spectral shape of the so obtained band can be quite complicated because of interference effect between the RIKES signal and the signal from non resonant OKE. We will talk about this problem in the framework of CARS spectroscopy.

Transient grating techniques

Third order nonlinear techniques are based on the interaction of four waves. The methods described above use two beams and involve a double interaction between the material and one of the beams. Therefore they have the drawback that they do not allow the individual control (polarisation, frequency, direction) of each wave. Such control is possible with the transient grating techniques, also called *four-wave-mixing* or *real time holography*. These techniques can be explained with either the holography or the nonlinear optics formalism.

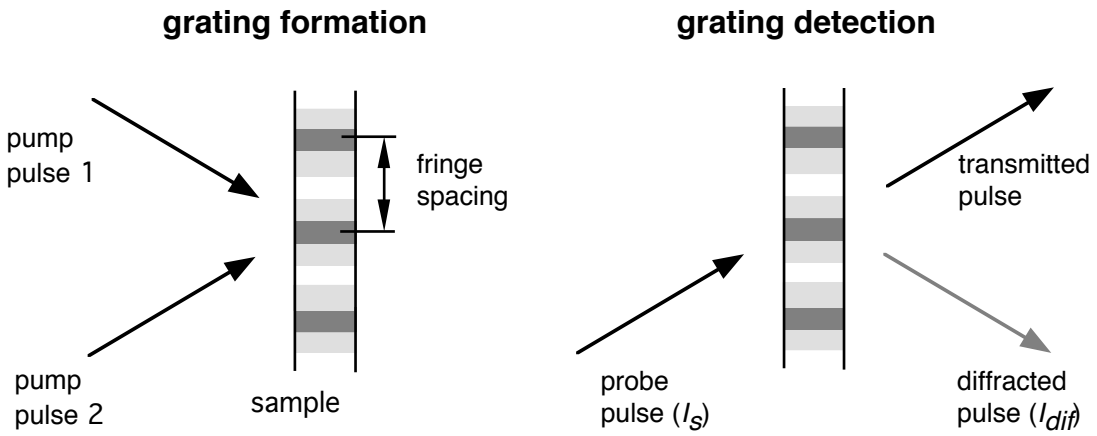

Figure 8.5: principle of the transient grating.

In the holography formalism, one distinguishes two steps (see **Figure 8.5**) :

1) **Grating formation :** the sample is excited with two time coincident laser pulses that cross on the sample. These two beams interfere and the light intensity on the sample is spatially modulated.

   If the light is absorbed (resonant case), there is a spatial distribution of ground and excited states populations. This results in turn to a spatial modulation of the optical properties of the sample. A periodic distribution of absorbance is equivalent to an amplitude grating, while such a distribution of refractive index is equivalent to a phase grating.

   If there is no absorption (non-resonant case), there can be a spatial distribution of refractive index due to optical Kerr effect or to electrostriction.

2) **Grating detection :** a probe laser pulse of intensity I_{pr} arrives on the sample with an angle of incidence equal to the Bragg angle, θ_B, and is partially diffracted. The intensity of the diffracted light, I_{dif}, is a function of the modulation amplitude of absorbance, ΔA, and of refractive index, Δn, at the probing wavelength, λ, and at time t :

$$\frac{I_{dif}(\lambda,t)}{I_s} \approx \left(\frac{\ln 10 \Delta A(\lambda,t)}{4\cos\theta_B} \right)^2 + \left(\frac{\pi L \Delta n(\lambda,t)}{\lambda \cos\theta_B} \right)^2 \qquad (8.4)$$

The modulation amplitude of absorbance is directly connected to the concentration of the different species absorbing at λ:

$$\Delta A(\lambda,t) = \sum_i \varepsilon_i(\lambda)\Delta C_i(t) \tag{8.5}$$

where ε_i is the absorption coefficient of species *i* and ΔC_i is its photoinduced variation of its concentration.

The variation of the refractive index can have various origins : population variation (Δn_p), density variation (Δn_d) and optical Kerr effect (Δn_{OKE}).

In the nonlinear optics formalism, the experiment is sensitive $\underline{\chi}^{(3)}\left(\omega_{dif} = \omega_s + \omega_p - \omega_p\right)$ and the diffracted signal intensity can be expressed as :

$$I_{dif} = \frac{\left(\mu_0/\varepsilon_0\right)^2}{16n^4}\frac{\omega_{dif}^2}{\varepsilon\left(\omega_{dif}\right)}\left|\chi_{ijkl}^{(3)}\right|^2 I_s I_{p1} I_{p2}\,\mathrm{sinc}^2\left(\frac{\Delta kL}{2}\right) \tag{8.6}$$

where the phase matching condition is :

$$\Delta k = \left|\vec{k}_{p1} - \vec{k}_{p2} + \vec{k}_s - \vec{k}_{dif}\right| = 0 \tag{8.7}$$

A typical geometry that satisfies this condition, which is equivalent to the Bragg condition, is shown in **Figure 6.2**.

The nonlinear susceptibility $\underline{\chi}^{(3)}$ can be expressed as a sum of contributions from population (*p*), density (*d*), electronic (*e*) and nuclear (*n*) optical Kerr effect :

$$\underline{\chi}^{(3)} = \underline{\chi}^{(3)}(p) + \underline{\chi}^{(3)}(d) + \underline{\chi}^{(3)}(e) + \underline{\chi}^{(3)}(n) \tag{8.8}$$

Each of these tensors has different symmetry properties and therefore, one can measure selectively each of these contributions by choosing the polarisation of the four waves.

Table 8.1: relative magnitude of tensor elements of various origins γ is the angle between the transition dipole involved in the pump process and the transition dipole involved in the probing process.

origin	$\chi^{(3)}_{1111}$	$\chi^{(3)}_{1122}$	$\chi^{(3)}_{1212}$	ζ
electronic	1	1/3	1/3	-71.6°
nuclear	1	-1/2	3/4	63.4°
population:				
γ= 0°	1	1/3	1/3	-71.6°
γ= 90°	1	2	-1/2	-26.6°
density	1	1	0	-45°

The relative magnitude of the various tensor elements is listed in Table 8.1. This table also gives the angle ζ, at which the contribution vanishes with the set of polarisation (ζ, 45°, 0°, 0°). For example, if the two pump beams are vertically polarised and if the probe beam is at 45°, the signal component polarised at ζ=-45° does not contain any density contribution.

Figure 8.6 shows the time profiles of the diffracted light intensity measured after excitation at 355 nm of a suspension of TiO_2 particules in water. The upper profile has been measured with all four waves polarised vertically and reflects $\chi^{(3)}_{1111}$, which contains contributions from $\chi^{(3)}_{1111}(p)$ and $\chi^{(3)}_{1111}(d)$. $\chi^{(3)}_{1111}(p)$ is due to the trapped electron population that decays by charge recombination. $\chi^{(3)}_{1111}(d)$ is due to the heat dissipated upon charge separation and recombination. The contribution of $\chi^{(3)}_{1111}(e)$ and $\chi^{(3)}_{1111}(n)$ can be neglected in this timescale.

The lower profile has been measured with the set of polarisation (0°, 90°, 0°, 90°) and thus reflects $\chi^{(3)}_{1212}(p)$.

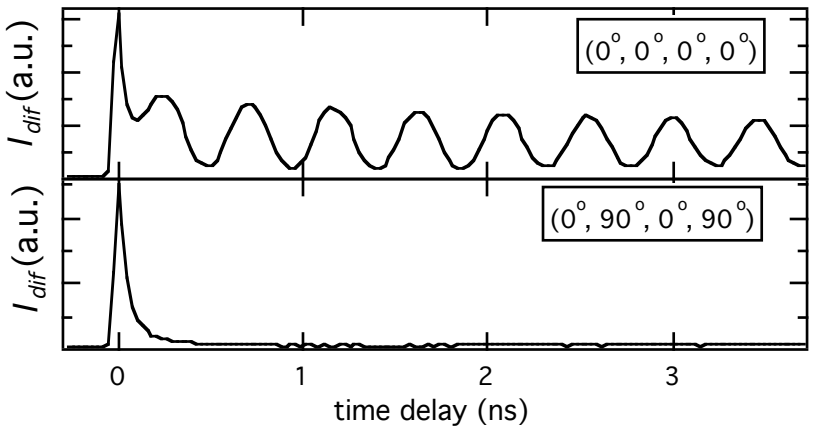

Figure 8.6: time profiles of the diffracted intensity at 532 nm after excitation at 355 nm of TiO_2 particules in water.

This transient grating techniques can be used to study a large variety of dynamic processes :

- *population dynamics* : measuring I_{dif} as a function of time and of λ gives information on the spectrum and the dynamics of transient species.
- *thermal processes* : Δn_d is mainly due to thermal expansion due itself to the energy dissipated during non-radiative transition or exothermic chemical processes. The measurement of Δn_d can be considered as a kind of time-resolved calorimetry. This technique can also be used to generate acoustic waves (laser ultrasonics).
- *Kerr effect* : one can work in non-resonant condition to measure Δn_{OKE}. By using the adequat polarisation, the electronic and nuclear contributions can be distinguished.

There are many other possible applications of these techniques.

CARS spectroscopy

CARS is the acronym of Coherent Anti-Stokes Raman Scattering. CARS spectroscopy is a third order nonlinear vibrational technique that is related to RIKES. An energy level scheme pertaining to CARS is shown in **Figure 8.7**.

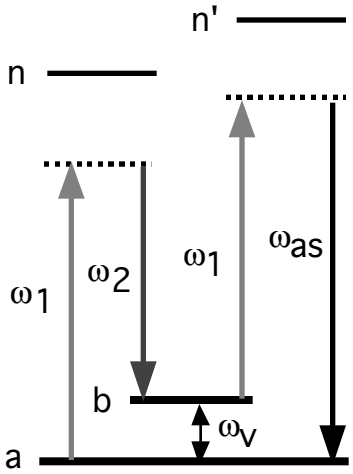

Figure 8.7: energy level scheme for CARS.

Practically, the sample is illuminated with two optical pulses at ω_1 and ω_2. If the frequency difference $\Delta\omega = |\omega_1 - \omega_2|$ corresponds to the frequency of a Raman active mode, ω_v, a signal at ω_{as}= $2\omega_1$ - ω_2, is generated.

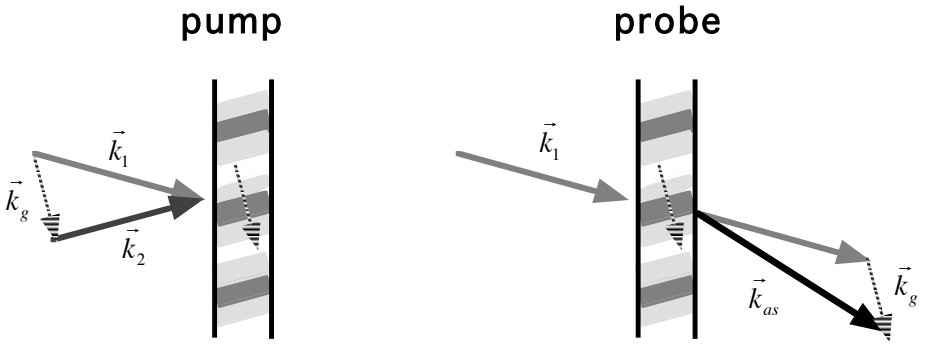

Figure 8.8: transient grating picture of CARS.

In a transient grating picture, one can show that the interference of two waves at ω_1 and ω_2 leads to a moving grating (non stationary interference pattern), with a beat frequency $\Omega = |\omega_1 - \omega_2|$. If this frequency is equal to a Raman active frequency, the moving electric field drives coherently the vibrational motion. In other words, all the molecules vibrate in phase. This coherent motion generates a modulation of refractive index moving at ω_{vib}.

A third pulse at ω_l striking this grating is diffracted in a well defined direction and its frequency is at $\omega_l \pm \omega_v$, the light at $\omega_l + \omega_v$ being the CARS signal.

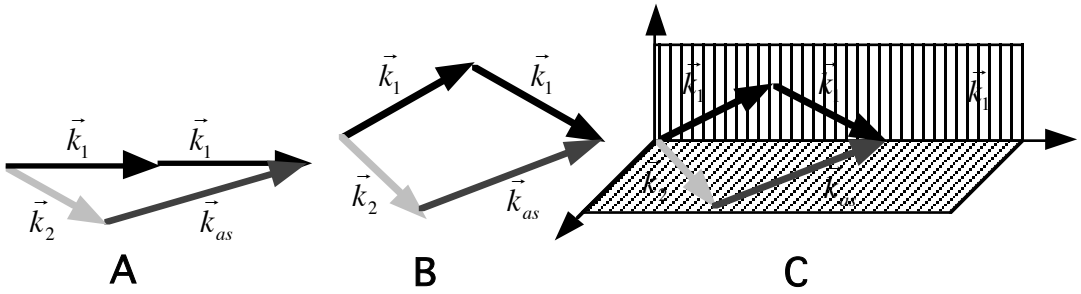

Figure 8.9: CARS geometries : A) general case, B) four-wave mixing geometry C) BOXCARS geometry.

The phase matching condition for CARS is :

$$\vec{k}_{as} = \vec{k}_1 + \vec{k}_r = 2\vec{k}_1 - \vec{k}_2 \tag{8.9}$$

where $\vec{k}_r$ is the grating wavevector. **Figure 8.9** shows some possible geometries for CARS.

A CARS spectrum is obtained by measuring the signal as a function of $|\omega_1 - \omega_2|$. The advantages of CARS over conventional Raman are :

- the CARS intensity is much larger and the signal propagates in a well defined direction. Thus the luminosity is larger by a factor 10^5-10^{10}.
- when working in electronic resonance, the CARS signal is not hidden by sample fluorescence.

The CARS intensity is similar to equation (8.6) with the corresponding tensor :

$$I_{CARS} \propto \left|\chi^{(3)}_{ijkl}(\omega_{as} = \omega_1 + \omega_1 - \omega_2)\right|^2 \tag{8.10}$$

The most important terms of $\underline{\chi}^{(3)}$ are those containing the resonance $\omega_{ab} - \omega_1 + \omega_2$ in the denominator :

$$\chi^{(3)}(R) = \frac{N}{\hbar^3}\frac{1}{\omega_{ab} - \omega_1 + \omega_2 - i\Gamma_r}$$
$$\times\sum_{n'}\left[\frac{\mu_{an'}\mu_{n'b}}{\omega_{n'a} - \omega_{as} - i\Gamma_{n'a}} + \frac{\mu_{an'}\mu_{n'b}}{\omega_{n'b} + \omega_{as} + i\Gamma_{n'b}}\right] \qquad (8.11)$$
$$\times\sum_{n}\left[\frac{\mu_{bn}\mu_{na}}{\omega_{na} + \omega_2 - i\Gamma_{na}} + \frac{\mu_{bn}\mu_{na}}{\omega_{na} - \omega_1 - i\Gamma_{n'b}}\right]$$

In resonant condition, $\omega_{ab} - \omega_1 + \omega_2 = 0$ and this term of $\underline{\chi}^{(3)}$ becomes very large.

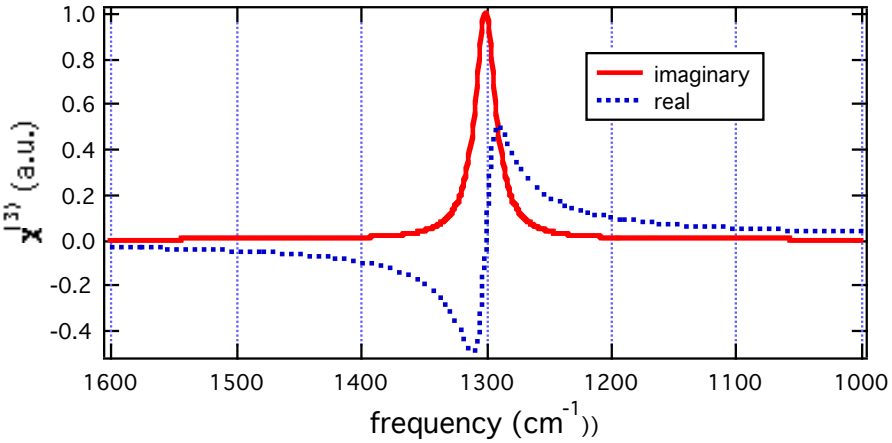

Figure 8.10: spectra of the real and imaginary parts of $\underline{\chi}^{(3)}(R)$ around a Raman resonance.

In general, one splits $\underline{\chi}^{(3)}$ into a non-resonant part (of electronic origin) and a Raman resonant part :

$$\underline{\chi}^{(3)} = \underline{\chi}^{(3)}(NR) + \underline{\chi}^{(3)}(R) \qquad (8.12)$$

As $\underline{\chi}^{(3)}(R)$ is resonant, it can be itself split into real and imaginary parts (see Figure 8.10):

$$\underline{\chi}^{(3)}(R) = \chi_r^{(3)}(R) + i\chi_i^{(3)}(R) \qquad (8.13)$$

The non-resonant part of $\underline{\chi}^{(3)}$ is purely real. The wave generated by the real part of $\underline{\chi}^{(3)}$ is dephased by 90° relatively to that generated by the imaginary part. Consequently, the CARS intensity is given by :

$$I_{CARS} \propto \left(\chi^{(3)}_{ijkl,i}(R)\right)^2 + \left(\chi^{(3)}_{ijkl,r}(R) + \chi^{(3)}_{ijkl,r}(NR)\right)^2 \qquad (8.14)$$

One can see that the real components of $\underline{\chi}^{(3)}$ interfere via the cross term $2\chi^{(3)}_{ijkl,r}(R)\chi^{(3)}_{ijkl,r}(NR)$. Consequently, the non resonant contribution amplifies the real part of $\underline{\chi}^{(3)}(R)$ to the detriment of the imaginary part. Therefore, the intense CARS lines are Lorentzian, while the weak lines have a dispersive shape.

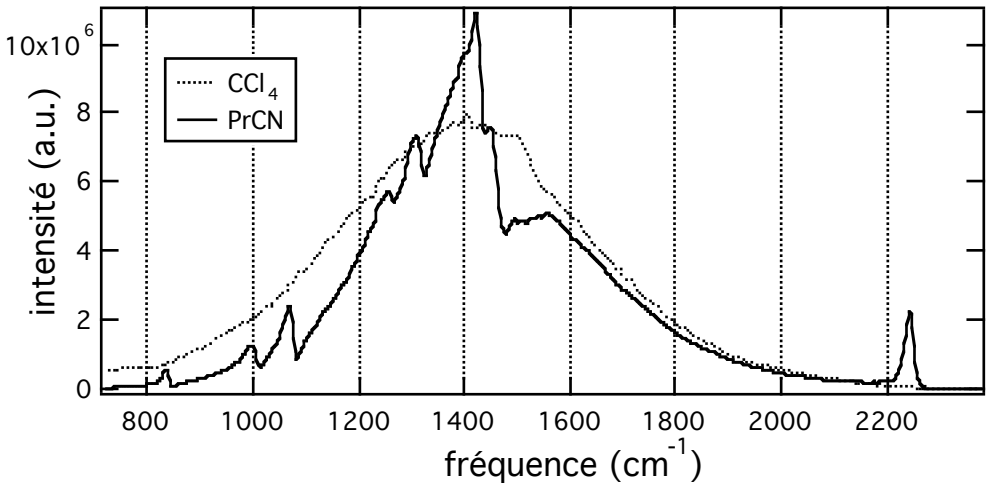

Figure 8.11: CARS spectra measured with laser pulses at 532 nm and at 560-590 nm.

Figure 8.11 shows two CARS spectra measured with a monochromatic pulse at ω_1 (532 nm) and a broadband pulse going from 560 to 590 nm.

In CCl_4, the signal originates from $\underline{\chi}^{(3)}_{NR}$ only. The gaussian shape of the spectrum is due to the geometry that was optimised to satisfy the phase matching condition for ω_2 (≈ 575 nm).

The CARS spectrum of propionitrile contains additionnally contribution from $\underline{\chi}^{(3)}_{R}$.

When $\underline{\chi}_R^{(3)} >> \underline{\chi}_{NR}^{(3)}$, the lines ares Lorentzian (~2300 cm^{-1}), while if $\underline{\chi}_R^{(3)} \approx \underline{\chi}_{NR}^{(3)}$, they are dispersive (~1500 cm^{-1}). Consequently, the precise determination of the vibrational frequencies requires a detailed lineshape analysis.

Conclusion

We have seen here only a few examples of $\chi^{(3)}$ type techniques. If one considers that these methods involve the interaction of four waves, one can realise the number of possible experiments. One can not only vary the frequencies and polarisation, but also the time and the duration of each interaction of light with the material. The understanding of most of these techniques requies a theoretical description of matter based on the density matrix formalism. This would go however beyond the scope of this short introductory course.

Further reading :

1) R. W. Boyd, *Nonlinear Optics*, Academic Press, London, 1992.

2) P. N. Prasad, D. J. Williams, *Introduction to Nonlinear Optical Effects in Molecules and Polymers,* J. Wiley, New York, 1991.

3) S. Mukamel, *Principles of Nonlinear Spectroscopy*, Oxford University Press, Oxford, 1995.

4) E. Vauthey, *Introduction to nonlinear optical spectroscopic techniques for investigating ultrafast processes,* Lectures of Virtual European University on Lasers, http://www.mitr.p.lodz.pl/evu/wyklady

5) W. W. Parson, *Modern Optical Spectroscopy,* Springer, Berlin, 2007.